Composite Structures 359 (2025) 118996

Contents lists available at ScienceDirect

Composite Structures

journal homepage: www.elsevier.com/locate/compstruct

Effect of prepreg ply thickness and orientation on tensile properties and damage onset in carbon-fiber composites for cryogenic environments

Eduardo Szpoganicz [a], Fabian Hübner [b], Uwe Beier [b], Matthias Geistbeck [b], Maximilian Korff [c], Ling Chen [d], Youhong Tang [d], Tobias Dickhut [c], Holger Ruckdäschel [a,*]

[a] Department of Polymer Engineering, University of Bayreuth, Bayreuth, Germany
[b] Airbus Central Research and Technology, Munich, Germany
[c] Department of Aeronautical Engineering, Chair of Composite Materials and Engineering Mechanics, University of the Bundeswehr Munich, Munich, Germany
[d] Institute for NanoScale Science and Technology, College of Science and Engineering, Flinders University, South Australia, Australia

ARTICLE INFO

Keywords:
CFRP composites
Ply thickness
Ply orientation
Cryogenics
Damage onset

ABSTRACT

This study addresses the effects of laminate design on the damage and failure behaviour of carbon-fiber reinforced composites with varying ply thicknesses and stacking configurations under cryogenic temperatures. The aim was to observe the ultimate tensile performance and in-situ onset of damage at 296 and 77 K environments, combining microscopy and simulation analyses. Laminates with fiber areal weights of 140, 70 and 45 g/m^2 were stacked in 2 different quasi-isotropic configurations. The results show that ultimate tensile properties are improved at 77 K, though failure strain slightly decreases. Thinner ply laminates with 70 and 45 g/m^2 showed a 15–20 % improvement in cryogenic tensile failure-strain, while damage onset shifted from 0.5 % to 0.8 % of strain. Adding off-axis plies improved laminates by 10–15 %, preventing damage onset up to failure. Microscopy and simulation analyses showed good agreement with the in-situ signal for the onset of damage, indicating matching levels of delamination failure initiation measured at 77 K. No transverse microcracks were observed, and permeation measurements showed no significant leakage increase after delamination onset. Ultimately, this work introduces a novel integrated approach by combining in-situ cryogenic testing, damage onset methodology, fractography, simulation analysis, and gas permeation measurements.

1. Introduction

The introduction of liquid hydrogen (LH2) as aircraft fuel has recently garnered attention for its potential to significantly diminish greenhouse gas emissions and reduce reliance on fossil fuels. LH2 is preferred for aircraft over gaseous hydrogen due to its higher energy density, which allows for more efficient storage and longer flight ranges. The in-flight discharge, as highlighted by the International Energy Agency (IEA), represents around 2–3 % of global energy-related emissions [1]. Noteworthy efforts by leading aircraft manufacturers are ongoing to advance technologies and conduct testing to introduce hydrogen-powered commercial aircraft [2]. Nevertheless, the widespread adoption of LH2 faces difficulties, particularly in storage, owing to the necessity for materials that can withstand extremely low temperatures (−253 °C) and effectively mitigate hydrogen leakage. LH2's inferior energy density compared to jet fuel requires larger storage capacities and results in weight increments, thus decreasing the storage/weight ratio of metallic tanks to commercial flights. Although carbon-fiber reinforced plastics (CFRPs) exhibit potential in combining structural integrity with a lightweight design, their performance in cryogenic temperature (CTe) remains constrained, giving rise to challenges as microcrack/damage onset and controlling leakage. Additionally, the complexity of testing methods and quantitative controls at < 77 K inhibits broad research adoption [3–5].

Initial investigation into design and evaluation was conducted already in 1973 by Chiao et al. [6]. The report evaluated integrity under cryogenic conditions via burst and liquid nitrogen (LN2) in-situ mechanical testing. Abumeri et al. [7], among other works from NASA, emphasized the critical need for reliable failure criteria in the cryogenic regime, which is essential for designing CFRP tank systems for future launch vehicles.

Aerospace-oriented studies reported the effect of thermal fatigue in FRP composites from a cryogenic range [8–13]. Results indicate that increasing the number of cycles and the temperature range increases

* Corresponding author.
E-mail address: holger.ruckdaeschel@uni-bayreuth.de (H. Ruckdäschel).

https://doi.org/10.1016/j.compstruct.2025.118996
Received 29 August 2024; Received in revised form 29 January 2025; Accepted 19 February 2025
Available online 21 February 2025

microcrack density. However, these studies conducted experiments using high-temperature epoxy matrix systems, such as Bismaleimide resin (high-temperature applications such as satellite materials). Consequently, the observation of microcracks in these materials is pronounced, and damage can be seen with clarity. Another important feature is that most of the research with microscopy analysis of crack and damage onset focuses on 0/90° cross-ply laminates, which is not a realistic laminate design for LH2 tanks, typically manufactured as multi-angled ply laminates, leading these results towards less applicability in practical use. Hydrogen tank stacking sequences typically use hoop layers for radial stiffness and helical or polar layers for axial stiffness, based on winding angles. For large-scale components, automated fiber placement (AFP) is used to achieve optimal fiber orientations for various load scenarios. Here, quasi-isotropic (QI) laminates are often used for material testing and engineering constants [14–16].

Numerous investigations have been focused on the mechanical properties of CFRP materials in cryogenic regimes [17–25]. The performance of T700 and T800 CFRP laminates at 77 K was reported by Wang et al. [17]. An increase in the tensile and compressive strength was reported in CTe environments. However, results on stiffness and strain to failure are not herein provided. Hohe et al. [18,19] performed static stiffness and strength tests in liquid helium (LHe, 4 K). Evidence was noted that in multidirectional laminates, the microscopic residual stresses observed at the single-ply level are further influenced by thermally induced residual stresses. These arise from the thermal mismatch between adjacent ply orientations. Furthermore, validation of Puck's failure criterion into the cryogenic regime showed that no loss in the overall stiffness can be observed. Szpoganicz et al. [20] investigated the impact of CFRP laminate ply thickness on interlaminar fracture toughness at 77 K. The study showed that using thinner plies through prepreg processing enhances delamination resistance and shear strength, particularly in CTe conditions. A 20 % increase in intralaminar energy release rate and shear strength for thinner plies was reported, emphasizing the heightened sensitivity to damage at 77 K environments. A further throughout survey on the mechanical properties of a CFRP composite was carried out in a low-temperature environment by Li et al. [21]. The research combined microscopic and macroscopic failure models to clarify the mechanical behaviour of the laminate. It was herein highlighted the embrittlement transformation and delamination damage at low temperatures.

Understanding CFRP behaviour in cryogenic temperatures remains unclear, posing challenges for developing dedicated CFRP composites for LH2 storage tanks. Hübner et al. [26,27] investigated enhancing epoxy resins for CFRP in cryogenic environments, finding that siloxane core–shell particles improved fracture toughness and fatigue crack propagation. Similarly, Qu et al. [28] reduced crack density in CFRP laminates by toughening the epoxy matrix with hydroxyl-terminated polyurethane (HTPU), enabling stress transfer to fibers even in cryogenic conditions.

Although major focus on the material design of CFRP storage tanks has been given to toughen the epoxy matrix, little attention has been given to the CFRP structure configuration, regularity, homogeneity and thus the effect of thinner plies. Sihn et al. [29] developed a new processing method for spreading fiber tows to make thinner ply CFRP laminates. The research investigated how reducing ply thickness affects the static and fatigue life of CFRP specimens in room temperature (RT) testing. Ultimately, it was found that thinner ply laminates alone can suppress microcracking, delamination, and splitting damage under static, fatigue, and impact loads without requiring special resin. Similar findings were provided by Amacher et al. [30], showing that the increase in structure regularity and decrease of major defects of thinner ply CFRP composites provided much better mechanical performance, and can expressively increase the tolerance for damage onset. Katsivalis et al. [5] investigated in detail the hydrogen permeability of thin-ply CFRP composites after mechanical loading and proved that no major leakage nor microcracks formation was found even after RT high tensile pre-loading (up to 1.4 % strain). Furthermore, intralaminar fracture toughness has been shown to vary with ply thickness and architecture in other literature studies [31–34]. Furtado et al. [31] found that the increase in notched strength with ply thickness is linked to the development of subcritical damage around the notch, which facilitates stress redistribution and reduces stress concentration. In a subsequent study, Furtado et al. [32] tested multidirectional laminates with ply thicknesses ranging from 67 μm to 268 μm under various loading conditions. It was reported an overall improvement in strength as ply thickness decreased. The referenced studies show significant improvements in CFRP materials' static and fatigue behaviour, which could greatly benefit laminates in LH2 storage tanks by reducing damage onset, evolution, and potential hydrogen leakage. However, these studies are conducted in RT environments and cannot be directly transferred to cryogenic conditions.

Targeting to further explore the effect of prepreg regularity and laminate design in CTe environments, this study investigated the effect of prepreg ply thickness and stacking configuration on tensile properties measured at RT and CTe environments. Three different prepreg ply thicknesses with the fiber areal weight of 140, 70 and 45 g/m^2, and two different QI configurations were manufactured with a toughened epoxy resin designed to operate in ultra-low temperatures. Tensile testing in LN2 was employed with a cryogenic-designed extensometer to monitor local strain, thus obtaining the ultimate tensile failure properties of these systems at RT and 77 K. Additionally, the extensometer could be adjusted so indicators of damage onset could be determined *in-situ* while tensile testing at 77 K. Scanning electron microscopy (SEM) was used to examine tensile specimens tested at various strain levels at CTe, to determine if the damage onset observed during tensile testing matched the strain levels where damage was visible in SEM after tensile loading. Furthermore, finite element modelling has been established to simulate the tensile behaviour of CFRP laminates under CTe environment for comparison with the obtained experimental results. Permeation tests on tensile specimens pre- and post-quasi-static loading at 77 K were carried out to search for a leakage-to-damage correlation. This comprehensive study aims to evaluate *in-situ* cryogenic tensile properties of CFRP laminates and identify critical laminate design factors influencing damage onset and properties for cryogenic storage tanks.

2. Materials and methods

2.1. Prepreg material

This study used aerospace-grade unidirectional carbon-fiber (HexTow® IMA 12 K) from Hexcel Corporation (Stamford, USA), impregnated with a cryogenic epoxy resin (CEP) designed for CTe environments. This reinforced composite is referred to here as CEP-IMA. The particulate toughening agent Genioperl W36® (Wacker AG, Burghausen, Germany) was added at 5 vol% to 100 parts of the matrix mixture. This siloxane-containing block-copolymeric toughener forms micelle-like core–shell structures in nanometer-sized, grape-like domains. Further details on the CEP resin can be found in Hübner et al. [26,27]. Prepreg tapes were produced using a hot-melt prepreg unit from Roth Composite Machinery (Steffenberg, Germany), with fiber areal weight of 45, 70, and 140 gsm, aiming for a 60 vol% fiber volume content (FVC). QI laminates were made from these tapes via autoclave curing at 130 °C. The prepreg tapes were consolidated into QI (Q1) laminates as $[0°,+45°,90°,-45°]_s$ to assess the effect of ply thickness alone. Additionally, a 45 gsm fiber areal weight laminate system was stacked as $[0°,+22.5°,+45°,+67.5°,90°,-67.5°,-45°,-22.5°]_s$ with off-axis orientations (Q2) to study the effect of ply orientation additional to the ply thickness. Details about the different laminate systems are shown in Table 1. Specimens were cut using an automated rotating blade machine Servocut 602 series from Metkon Instruments Inc. (Bursa, Turkey), ensuring defect-free cuts. Thermogravimetric analysis (TGA) using a TG 209 F1 Libra from Netzsch-Geraetebau (Selb, Germany)

Table 1
Summarized details about the different QI laminate systems design.

Laminate	Laminate thickness / fiber gsm / FVC			Stacking sequence	*n* of plies
140-Q1	2.1 ± 0.2 mm	140	61 ± 4	$[0°/+45°/90°/-45°]_{2s}$	16
70-Q1	1.8 ± 0.1 mm	70	60 ± 1	$[0°/+45°/90°/-45°]_{3s}$	24
45-Q1	1.9 ± 0.2 mm	45	58 ± 1	$[0°/+45°/90°/-45°]_{5s}$	40
45-Q2	2.0 ± 0.1 mm	45	58 ± 1	$[0°/+22.5°/+45°/+67.5°/90°/-67.5°/-45°/-22.5°]_{3s}$	48

monitored the FVC according to DIN 16459:2019–12 standard [35]. The TGA test was conducted under controlled heating conditions, with a temperature range of 25 to 1000 °C at a heating rate of 20 °C/min. Initially, the test was performed in an O2 atmosphere up to 600 °C to eliminate the degraded polymer matrix, followed by a transition to an N2 atmosphere.

2.2. Tensile testing and damage onset

Tensile testing was carried out using a 100 kN universal testing machine, adapted for cryogenic testing, from Franz Wohl + Partner Prüfmaschinen GmbH (Schalkau, Germany). A tailored polytetrafluoroethylene mould for containing the test environment at 77 K (*in-situ* with LN2) was designed for 2 mm thick specimens. The mould is sealed underneath with a silicon seal before every testing, to ensure that LN2 is not leaked at the tabs-cavity. An illustrative and schematic view of the adapted test can be seen in Fig. 1.

The characteristics of the test and of the specimens was carried out according to ASTM D3039 [36]. An axial extensometer designed to operate in LN2 from Sandner Messtechnik GmbH (Biebesheim am Rhein, Germany) was used to record the local strain *in-situ* of the CFRP specimen up to failure. The use of Invar alloy in selected parts of the sensor minimizes the interference caused by the thermal contraction of its components. Here, sharper blades are recommended to ensure the sensor remains steady when immersed in boiling LN2. The sensitive extensometer also allows for gradual levels of attachment, enabling the detection of strong vibrations, which were later associated with damage onset and confirmed through microscopy analysis.

2.3. Microscopy analysis

To further understand damage initiation, multiple levels of mechanical loading were applied to the laminate systems and further analyzed in an SEM from Zeiss Gemini 1530 (Oberkochen, Germany). Surfaces were platinum-sputtered to 5–10 nm thickness before examination, with the SEM operating at 3 kV. For each of the CFRP systems, three incremental tensile-strain levels (0.2 %, 0.5 %, and 0.8 %) at CTe were applied, selected based on tensile test results identifying these values as critical onset points. The tensile loading setup followed that described in Fig. 1. After applying each strain level, specimens were prepared for SEM analysis to identify microcracks and delamination damage, enabling direct comparison between SEM images and tensile levels of strain recorded during tensile loading at 77 K. Notice that SEM analysis is carried out at RT.

2.4. Simulation analysis

The geometric modelling of the laminates consisted of CFRP representative multiple plies and cohesive elements. The stacked plies, shown in Fig. 2**a**, were built in accordance with each system as done experimentally (see Table 1). The cohesive elements, which have zero thickness, were introduced by inserting cohesive seams into the mesh module in each ply. The element types for the plies, cohesive elements, and tabs were C3D8R, COH3D8, and C3D8R, respectively. The element sizes for the plies, cohesive elements, and tabs were specified as 1 mm, 1 mm, and 2.5 mm, respectively, as shown in Fig. 2**b**. The normal and shear stiffness coefficients of the cohesive elements were calculated to match the equivalent transverse normal and shear stiffness of the continuum material. The material properties utilized to compute the simulation analysis are summarized in Appendix A. Here, ABAQUS software was utilized for the simulation analysis.

To simulate the damage evolution process of the laminate during tension, the 3D Hashin criterion was applied via VUMAT. This criterion was selected because it is suitable for describing the multi-failure mode behaviour of fiber composites, including four failure mechanisms: fiber tension, fiber compression, matrix tension and matrix compression, and thus it is applicable to anisotropic structures [37–39]. The 3D Hashin criterion is used as a failure criterion to simulate the damage evolution process of laminated panels. It includes four different failure modes: fiber tensile **Eq. (1)**, fiber compression **Eq. (2)**, matrix tensile **Eq. (3)**, and matrix compression **Eq. (4)**:

Fiber tensile failure ($\sigma_{11} \geq 0$) :

$$F_{ft} = \left(\frac{\sigma_{11}}{X_T}\right)^2 + \alpha\left(\frac{\sigma_{12}}{S_{12}}\right)^2 + \alpha\left(\frac{\sigma_{13}}{S_{13}}\right)^2 \geq 1 \quad (1)$$

Fiber compression failure ($\sigma_{11} \leq 0$) :

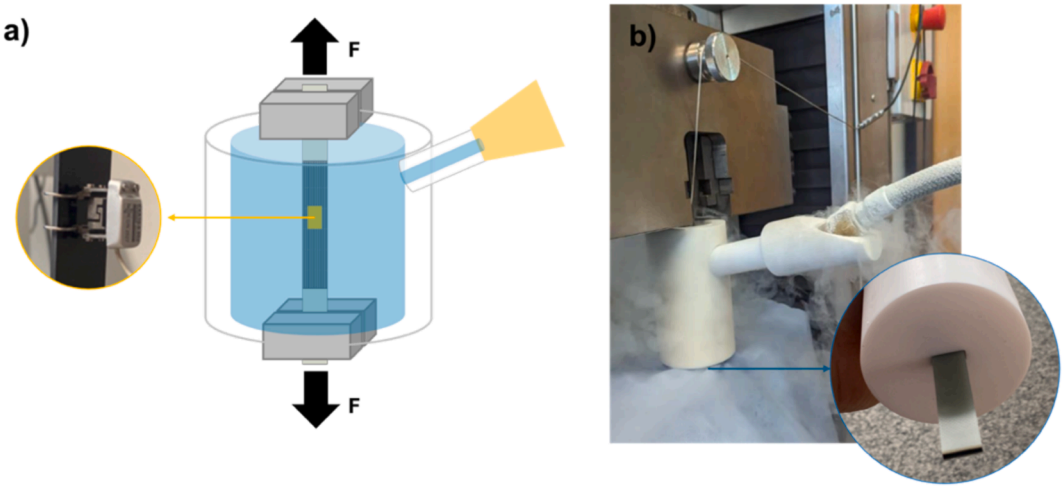

Fig. 1. A) illustration and b) schematic view of *in-situ* LN2 tensile testing with adapted extensometer strain-gauge and PTFE container.

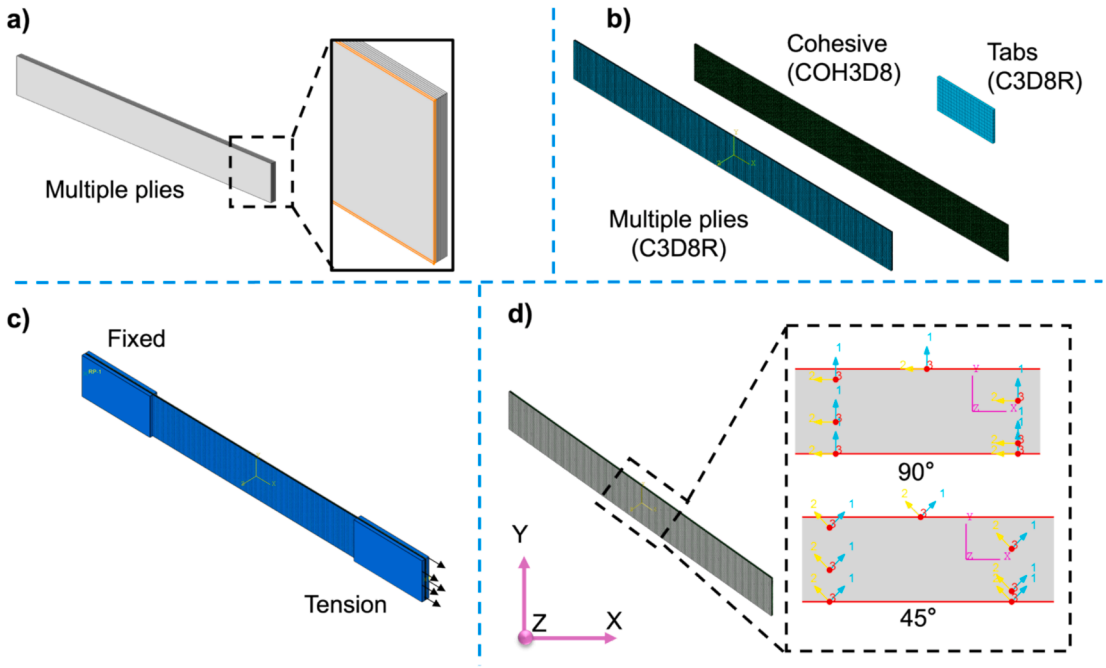

Fig. 2. Finite element modelling of laminate. a) The 3D structure diagram of multiple plies, b) inserting cohesive and meshing units, c) tension boundary condition and d) defining ply direction.

$$F_{fc} = \left(\frac{\sigma_{11}}{X_C}\right)^2 \geq 1 \tag{2}$$

Matrix tensile failure ($\sigma_{22} + \sigma_{33} \geq 0$) :

$$F_{mt} = \left(\frac{\sigma_{22}+\sigma_{33}}{Y_T}\right)^2 + \frac{1}{S_{23}^2}\left(\sigma_{23}^2 - \sigma_{22}\sigma_{33}\right)\left(\frac{\sigma_{12}}{S_{12}}\right)^2 + \left(\frac{\sigma_{13}}{S_{13}}\right)^2 \geq 1 \tag{3}$$

Matrix compression failure ($\sigma_{22} + \sigma_{33} \leq 0$) :

$$F_{mc}{}^2 = \left[\left(\frac{X_C}{2S_{23}}\right)^2 - 1\right]\frac{(\sigma_{22}+\sigma_{33})}{Y_C} + \frac{(\sigma_{22}+\sigma_{33})^2}{4S_{12}^2} + \frac{\sigma_{23}^2 - \sigma_{22}\sigma_{33}}{S_{23}^2} + \frac{\sigma_{12}^2+\sigma_{13}^2}{\sigma_{12}^2} \geq 1 \tag{4}$$

where σ_{ij} (ij = 1,2,3) is the effective stress component; X_T and X_C are longitudinal tensile and failure strengths; Y_T and Y_C are transversal tensile and failure strengths; and S_{12}, S_{13} and S_{23} are shear failure strengths. Further details can be seen in [37]. Although the Hashin criterion is suitable for predicting global damage onset on the specimen, it may not capture detailed failure modes; alternatives like the Puck criterion can offer more detailed in failure analysis.

The explicit dynamic analysis step was selected, and the geometric nonlinearity option was activated to account for large deformation effects. One end of the laminate was completely fixed, while the other end was stretched, as shown in Fig. 2**c**. A coordinate system was used to set the angle of each plane, with '1′ representing the axial direction of the fiber, and '2′ and '3′ representing the transverse directions. To ensure consistency with the experimental conditions, the boundary conditions of the simulation involve the application of displacements. The four tabs are first tied to the surface of the laminates, with the left two tabs coupled to a reference point that is fully fixed. Displacements (0.3, 0.75, 1.2, 1.5, and 1.8 mm) are applied to the right two tabs, calculated by multiplying the strain values (0.2 %, 0.5 %, 0.8 %, 1.0 %, and 1.2 %) by the specimen's span length of 150 mm. Fig. 2**d** shows the angles of the planes, including 90° and 45°. The critical tensile and shear stresses of the cohesive law were matched to the transverse tensile strength and in-plane shear strength of the UD plies. The uncoupled normal and shear stiffness coefficients of the cohesive elements were calibrated to be equivalent to the continuum transverse normal and shear stiffness. Additionally, interlaminar cohesive interfaces were modelled similarly, utilizing experimentally determined fracture energies in mode I and II, and interlaminar shear strength ILSS (obtained in [20]). Thermal residual stress is not included in the simulation herein, as ABAQUS usually do not support thermal–mechanical coupling element type, driving the focus primarily for modelling interface strength, separation, and crack propagation.

2.5. Permeation & leakage

Permeation measurements were conducted according to ASTM D1434-82 standard [40] using a monometric system employing the closed volume and variable pressure method. Leakage through the CFRP material was determined using a mass spectrometer system. Permeation and leakage measurements were taken at RT with helium gas. Tensile bars, adapted from the ASTM D3039 specifications, served as the test specimens, allowing for the evaluation of CFRP system permeation and leakage both before and after subjecting the material to tensile loading in CTe environments. The leakage channel contains a transversal area of 1592 mm^2 area. To ensure that the adapted tensile specimens fully covered the area of the leakage channel, the width of the tensile specimen was increased from the original 25 mm to 55 mm. Initially, permeation measurements were taken on the tensile bars prior to applying any load. Subsequently, the specimens were submitted to a 0.8 % tensile strain at 77 K, following the testing method of **Section 2.2**. The strain was chosen based on the tensile results described in **Section 3.1**. Finally, the loaded specimen was once again tested, and values were compared as prior to loading (unloaded specimen) and after loading (loaded specimen). A schematic view of the testing concept is shown in Fig. 3.

2.6. Matrix of tests

In this section, a comprehensive matrix detailing all the tests conducted during this survey is presented. This matrix serves as an organized framework to summarize the extensive range of experimental and analytical evaluations performed on the composite materials. The

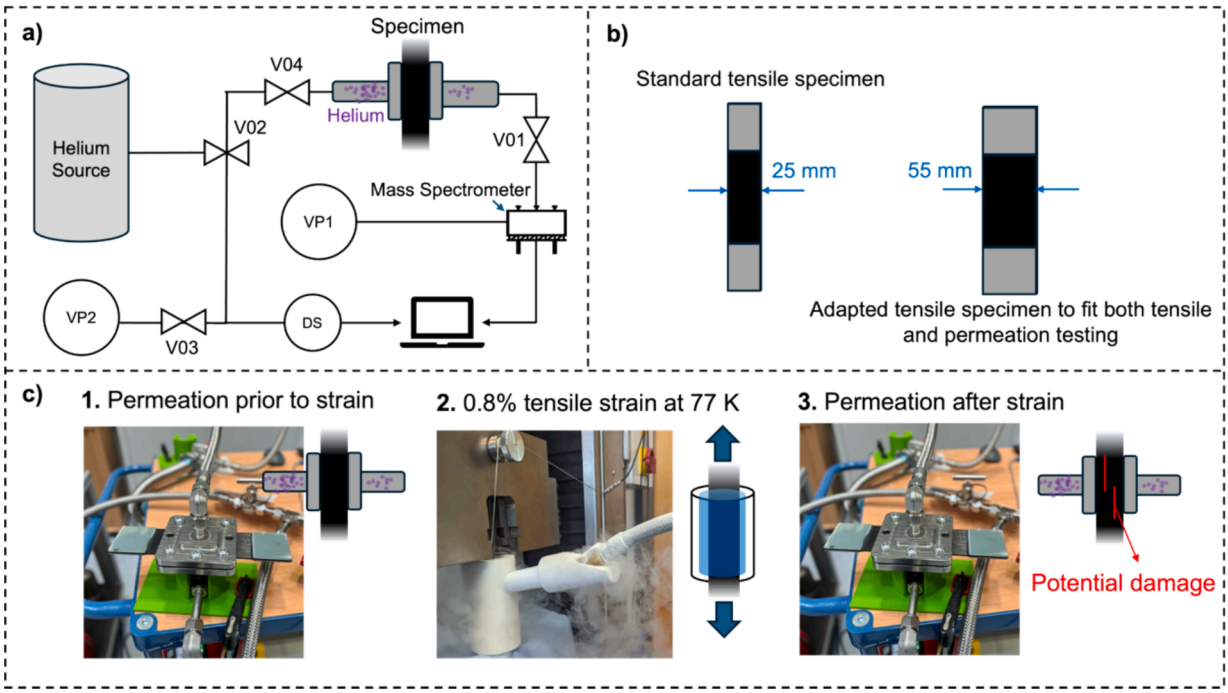

Fig. 3. Schematic representation of the permeation-to-damage survey, as the illustration of a) the testing rig, b) the adaptation of the tensile specimens to fit the permeation channel area, and c) the sequential methodology for this survey.

Table 2
Summarized matrix of methods and objectives for each section of this work.

Section	Procedure	Objective	Specimens
Prepreg material	Manufacture prepreg tapes with varying fiber areal weights (140, 70, and 45 gsm).	Obtain prepregs with varying fiber–matrix regularity and stacking configuration.	–
Tensile testing & damage onset	Perform tensile testing up to failure in RT and CTe environment.	Obtain information about tensile properties measured *in-situ*.	5 Specimens for each system.
	Perform tensile testing up to failure in CTe environment with adjusted extensometer.	Obtain information about damage onset measured *in-situ*.	3 Specimens for each system.
Microscopy analysis	Perform SEM analysis of damage on tensile specimens subjected to 0.2, 0.5, and 0.8 % strain in CTe environment.	Correlate damage onset visualized in SEM and from *in-situ* tensile testing.	3 Specimens of each system for each load step.
Simulation analysis	Perform FE modelling of experimentally tested laminate designs subjected to 0.2 % to 1.2 % tensile strain in CTe environment.	Correlate simulated damage initiation and progression with *in-situ* tensile testing.	1 model for each system for each load step.
Permeation & leakage	Perform permeation and leakage measurements of widened tensile specimens before and after applying 0.8 % tensile strain in CTe environment.	Observe the effect of damage onset on permeation and leakage properties.	1 Specimen for each system.

schematic summary is shown in Table 2.

3. Results and discussion

3.1. Tensile properties

All four CFRP systems were characterized by tensile load up to failure. The QI specimens utilized herein were stacked according to Table 1. The stress and strain measured in ambient (RT representative) and *in-situ* LN2 (CTe representative) are shown in Fig. 4**a** and Fig. 4**b**, respectively. Overall, the elastic modulus is not affected by the improvement on the structure regularity nor the stacking configuration. When considering the classical laminate theory (CLT), a symmetric QI laminate should have identical stiffness regardless of the ply thickness. Considering a dominant mode of failure as crack propagation as the Griffith theory of fracture, the laminate strength σ_S is inversely proportional to the square root of the characteristic size of the crack a, as shown in **Eq. (5)**:

$$\sigma_S = \sqrt{\frac{E\, G_{IC}}{\pi\, a}} \tag{5}$$

Where E stands for the elastic modulus and G_{IC} the critical strain energy release rate.

When intralaminar damage is constrained by the surrounding plies, the crack size is equal to the ply thickness [41–43]. Thus, suggesting that thinner plies confine smaller cracks, and therefore higher failure strength. At RT testing, the tensile failure of all laminates followed similar behaviour, suggesting no expressive advantage of thinner plies. The cryogenic-tailored epoxy resin CEP permits a large plastic radius zone for deformation to occur at RT (details in Hübner et al. [26]), which is believed to cover the many irregularities seen for thicker laminates. Contrary to what is observed in works using typical brittle resins [29,30], where significant enhancement is seen at RT, the irregularities of thick-ply features such as resin-pockets and fiber weaving do not appear to be critical for the CEP-IMA laminate at RT. Additionally, the low cure-temperature resin CEP is expected to have significantly lower residual stress compared to high T_g systems when bringing the laminate to RT. Overall, the systems behave similarly, except the 45-Q2 laminate,

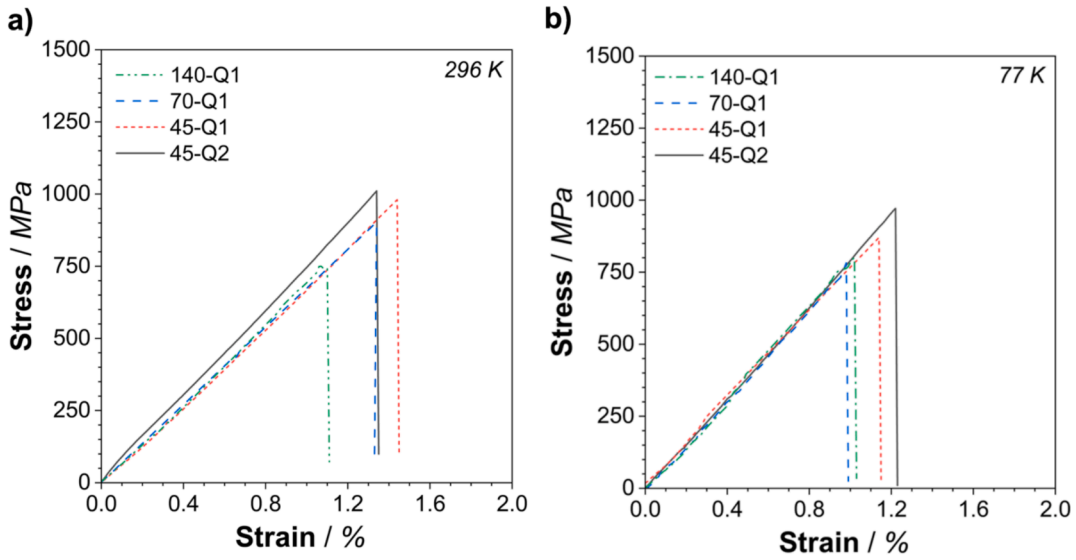

Fig. 4. Representative stress–strain tensile curves of the CEP-IMA laminates measured at a) 296 K and b) 77 K environment.

which shows a slight increase in stress-failure. This can be attributed to the optimized residual stress–strain, influenced by the reduction of ply angle, also reported by [30].

In CTe environments, the strain-failure was steadily improved when decreasing the ply thickness, especially when additionally containing the off-axis ± 22.5° and ± 67.5° fiber orientation (from 0.98 % to 1.21 % strain failure). Thus, the strength of the material is reported much higher accordingly (from 749 MPa to 942 MPa). The observed enhancement highlights a significant increase in sensitivity to irregularities and vulnerable areas, particularly noticeable in thicker prepregs. Due to the substantial reduction in the plastic zone radius at CTe factors that may have been considered negligible at RT become critically important (e.g. for LH2 tanks). Such a phenomenon is well documented in [20,27]. This sensitivity growth found at 77 K correlates with the larger strain levels of failure found for the 45 gsm laminates. The even further improved performance of the off-axis CFRP laminate CEP-IMA 45-Q2 can be attributed to the management of residual stresses within the CFRP laminate. When considering the temperature change from the curing temperature (403 K for the CEP-IMA composite) to the CTe environment (77 K), it is encountered a significant temperature range of 326 K. In composite laminates, the inter-ply regions, which typically contain excess resin from the prepreg tape processing, play a crucial role. The placement of higher angles between adjacent plies results in increased induced stress within the laminate structure. By steadily changing the ply orientations, the laminate can effectively distribute stress concentrations, and the thermal stress is far less concentrated at the ply interface, ultimately leading to enhanced durability when loading at CTe. The summary of the properties measured in RT and CTe are presented in Table 3.

Table 3
Summary of tensile properties measured at RT and CTe for all systems.

CFRP system	E Modulus / *GPa*		Stress Failure / *MPa*		Strain Failure / %	
	296 K	77 K	296 K	77 K	296 K	77 K
140-Q1	61 ± 2	68 ± 3	773 ± 28	749 ± 99	1.13 ± 0.02	0.98 ± 0.07
70-Q1	63 ± 1	70 ± 2	934 ± 35	805 ± 14	1.35 ± 0.01	0.99 ± 0.01
45-Q1	61 ± 1	68 ± 1	910 ± 27	878 ± 33	1.34 ± 0.03	1.13 ± 0.05
45-Q2	63 ± 2	69 ± 5	1035 ± 57	942 ± 62	1.31 ± 0.03	1.21 ± 0.03

3.2. Damage onset via in-situ testing

To view the onset of damage within the CFRP laminates, a representative curve of each system measured at 77 K, given the original curve (including the signal shift caused by the damage) and the normalized curve (removing the signal shift caused by the damage) was plotted in Fig. 5. The normalized curve is a projection from the original curve baseline (based on a linear regression) prior to the signal shift caused by the damage. As already reported by Hohe [19] on the validation of Puck's failure criterion for CFRP at CTe environments, the damage on the laminates does not exhibit a significant loss in the material stiffness. Furthermore, experimental studies suggest that crack formation and stiffness degradation are significantly delayed in thin plies due to their confinement between stiffer neighbouring plies [44–47]. Thus, suggesting that the slope of the curve is maintained even after damage occurred. Therefore, it is understood that a linear regression is appropriate in this context.

The tensile performance of the QI laminates generally involves multiple damage events. The matrix cracking within the 90° plies, as intra-laminar transverse cracking, is thought of as the event wherein damage onset takes place. When evaluating the 140-Q1 in 77 K, a strong signal shift was detected always within the range of 300–400 MPa of stress and 0.4–0.5 % strain, likely indicating the failure of the 90° plies. The anticipated failure can easily progress to the adjacent plies as intra-laminar shear damage, and thus cause the material to fail significantly earlier, as also reported by [30]. Multiple signals of damage onset were always reported for the 140-Q1 laminate. The free edge effect, for instance, occurs due to stress concentrations at the edges where there is reduced restraint from neighbouring plies, making these regions more susceptible to delamination. Additionally, hydrostatic stress dominant suppresses the plastic deformation (e.g. cleavage) as a result of triaxiality. Thicker cross-plies worsen this effect as they increase the distance between adjacent plies, leading to greater stress gradients and a higher likelihood of cohesive failure.

The tensile specimens are far more sensitive to this in CTe environments, as the plastic zone radius of the matrix and the delamination toughness of the laminate decreases substantially. The 70- and 45-Q1 laminates exhibited a higher damage onset, only being detected at the range of stress 600–750 MPa and strain 0.7–0.8 %. Here, the significant improvement in structure regularity and reduction of the cross-ply crack size is believed to be the reason for such an increase in the stress at damage onset. The distribution of damage permits the adjacent plies to withstand longer to the stress–strain load. Likely reducing delamination

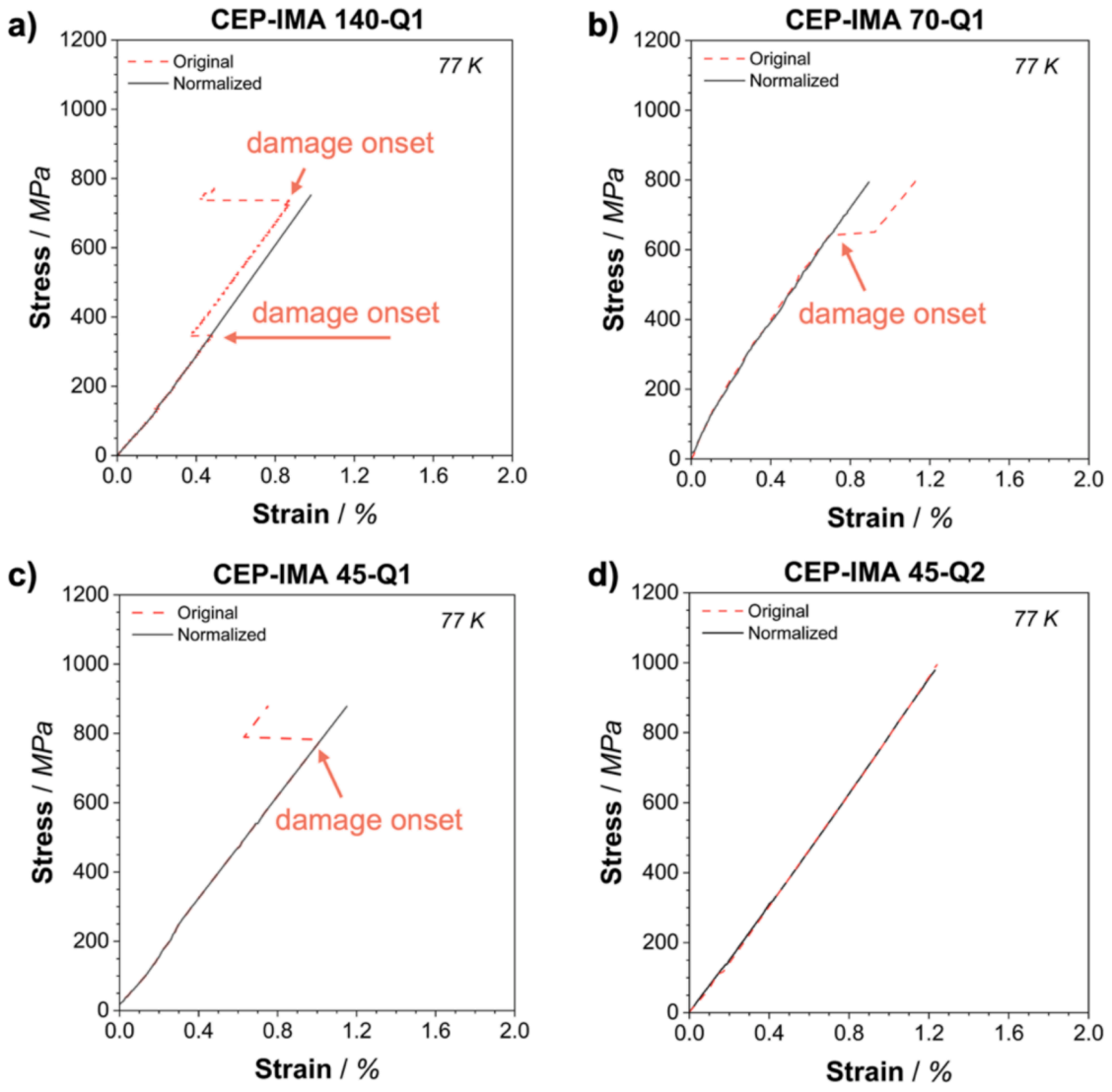

Fig. 5. Representative stress–strain curves of the different CEP-IMA laminates measured at 77 K exhibiting the original curve containing the extensometer signal shift and the normalized curve as a) 140-Q1, b) 70-Q1, c) 45-Q1, d) 45-Q2.

area and shifting ultimate failure towards higher stress–strain. The shift of damage onset towards higher tensile stress–strain values should be related to the stability of transverse intra-laminar crack. However, the residual stress caused by the extreme environment and large angled plies (90°/45°/0°) still seems to take a major role in damage onset. As the magnitude of the damage is proportional to its size, the drastic reduction on the ply interface and the final failure is likely to follow asymptotic behaviour. Therefore, a further increase is seen when reducing the ply thickness of Q1 from 70 to 45 gsm. All 70- and 45-Q1 specimens exhibited damage in the range of 0.7–0.8 % strain.

Moreover, no sign of damage prior to ultimate failure was found for the 45-Q2 laminates. As important as structural regularity is, the onset of damage caused by residual stress plays a key role. As the Q2 laminates contain additional ± 22.5° and ± 67.5° plies, the variation between curing temperature (408 K) and CTe (77 K) causes less residual stress as the ply angle is reduced when compared to Q1. When designing composites for LH2 tanks, where cracks are a critical factor, ensuring complete resistance to damage initiation (whether from cracks or delamination) is far more important than merely delaying their onset. Therefore, designing a laminate that can prevent cracks and delamination (such as Q2) during its use would significantly benefit LH2 tank design. Based on the results herein, the structural regularity of 90° ply thickness reduction can have significant improvements on the ultimate stress–strain of the CFRP laminate. Still, it is only by reducing the plies angles that residual stress in 77 K is believed to be controlled, and the onset of damage can be prevented. Fig. 6 exhibits the fractography of the in-situ tested specimens (77 K) and clearly indicates that, reducing ply thickness and incorporating off-axis stacking configurations in CFRP results in more homogeneous material behaviour, promoting a more

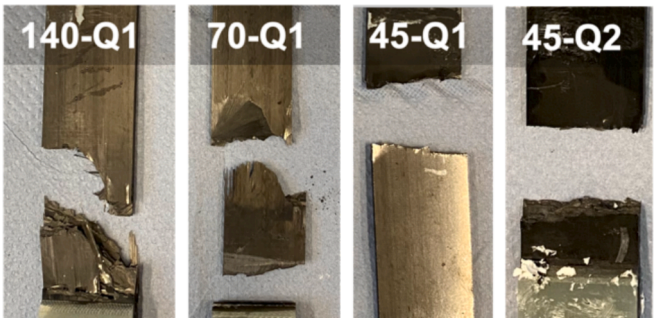

Fig. 6. Tensile failure modes observed for QI laminates tested in cryogenic environments.

monolithic failure. This was a common observation within all tested specimens.

In Fig. 7, a plot has been made comparing the CTe ultimate stress–strain failure of the laminates and the observed strain at damage onset. By analysing the graph, it is observed that reducing the ply thickness results in an upward shift of both the ultimate failure and damage onset to higher strain values. However, it is only through decreasing the ply angles that damage onset matches the ultimate failure of the material. The onset of damage significantly influences the fatigue properties of CFRP materials, as shown in [29]. If the damage onset is shifted towards higher strain values, the material can withstand greater loads for a longer duration, enhancing the reliability and longevity of LH2 storage tanks. Conversely, an earlier onset of damage, as for 140-Q1, could result in a much shorter fatigue life as soon as damage onset is encountered. As fatigue life highly depends on damage onset, eliminating/delaying damage onset, as for 45-Q2, would greatly improve the durability of LH2 CFRP storage tanks.

3.3. Damage onset via SEM analysis

To support the damage onset method, a survey was carried out with the CFRP laminates, submitting the accordingly specimens to 0.2 %, 0.5 % and 0.8 % of tensile strain at 77 K and subsequently analysed in SEM. Fig. 8 exhibits the cross-section of the laminates after the progressive tensile strain in CTe. In Fig. 8**a**, no sign of damage was observed at 0.2 % tensile strain. Likewise, the stress–strain curves measured at 77 K never exhibited signs of damage at this stage.

The SEM images of the laminates after a 0.5 % tensile strain in CTe are shown in Fig. 8**b**. At this strain level, only the 140-Q1 specimens exhibited matching signal shifts in the *in-situ* tensile testing and within the SEM images. The pictures were able to reveal delamination spots through the 140-Q1 laminate at this stage. At this strain range, part of the 70-Q1 specimens showed signs of damage onset through the signal shift. However, when searching for damaged spots through the SEM images, no transversal cracks nor delamination could be found. A possible explanation for this is that the material is indeed not yet damaging, but instead the glue between the specimen and the tabs. This could also cause a signal shift. Also, the SEM analysis conducted at RT presents a challenge in detecting minor cracks, as the resin undergoes volumetric expansion when transitioning from CTe to RT and can cover minor signs of damage.

At a strain of 0.8 %, noticeable signal shifts were observed in all Q1 samples, while none were detected in the Q2 samples. These onset signals matched the observed SEM images shown in Fig. 8**c**. These delamination sites were predominantly evident within the 90° cross-ply region, with clearer manifestations in the 140 gsm samples, some of which were perceptible to unaided vision. Conversely, delamination sites in the 70- and 45-Q1 samples were less pronounced, yet still critical, while no cracks were discernible in the 45-Q2 laminates. Although close examination of certain images for the 45 g/m^2 laminate revealed subtle indications of damage, distinguishing between damage spots from the material defects and imperfections remained challenging. Thus, assuming no damage onset to this system until its failure. Consequently, an estimated threshold for the onset of damage in 77 K was established as 0.5 % strain for the 140-Q1 laminates, 0.8 % for the 70- and 45-Q1 laminates, and 1.2 % (ultimate failure) for the 45-Q2 laminates, aligning with the trends observed in Fig. 5. Ultimately, the cryogenic-design resin CEP proven to be resistant against transversal microcracks, as a result from sufficient elongation to effectively transfer the stress to the fibers even at CTe. Instead, delamination was the primary mode of damage, localized within the 90°/±45° plies. For thin-plies and especially ultra-thin plies, literature reports show a similar trend of damage mechanism. Wagih et al. [48] studied damage sequences in thin-ply CFRP laminates during a RT impact event. Results showed that for ultra-thin ply laminates, the first damage mechanism to appear is delamination. Similarly, Sihn et al. [29] observed that as the number of plies increases and ply thickness decreases, there is a tendency for overall microcracking and delamination to decrease, with microcracking being suppressed at a higher rate.

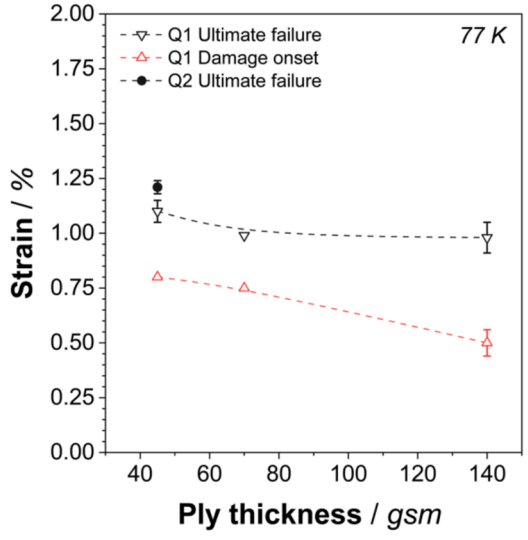

Fig. 7. Ultimate strain failure and onset of damage at 77 K as a function of the ply thickness.

3.4. Simulation analysis

3.4.1. Interlaminar damage via cohesive surface

In Fig. 9, it is possible to see the interlaminar damage progression in the different tensile strain (from 0.2 % to 1.2 %) for all different ply thickness laminates under cryogenic conditions. An increase in stress at the cohesive surface (e.g. 90°/+45° or 90°/+67.5°) leads to the onset and growth of damage at the crossply interface. When observing micromechanics of tensile failure [41–43], the 90° ply interface is often emphasized due to its critical role in damage initiation and propagation under longitudinal tensile loading. This interface is prone to shear-induced delamination. Thus, being the focus of study herein.

Delamination spots appeared to be triggered by local stress concentrations at the tabs and free edges, propagating further as the strain level increased. The image clearly shows that thicker ply materials start delamination failure early already at a strain level of 0.5 %, thus matching the experimental results. Delamination grows sequentially as the strain level increases, with the dissemination of damage appearing much rougher compared to thinner ply systems, shifting the cohesive failure towards higher loads. The 70-Q1 thin-ply material shows an improvement in stress distribution, raising the onset of cohesive failure to a strain level of 0.8 %. The 45-Q1 thin-ply exhibits a similar effect but at even higher strain conditions. For the off-axis stacking configuration of 45-Q2, delamination damage is not detected below 1.2 % of strain. The Mises Stress indicates the regions susceptible to stress and yielding given the tensile strain. As the stress increases, signs of damage and failure within the material are seen more expressive, suggesting, for example, the onset of delamination or crack propagation along the interface. Ultimately, the graph suggests that the stacking configuration significantly affects stress transfer, reducing and distributing concentrated stress, and consequently minimizing interlaminar damage within the composite. This is especially important in CTe environments, where embrittlement takes place. Although a continuous part (such as a storage tank) may not exhibit free edges, boss and dome areas might also be susceptible to stress concentration, thus encouraging this concept. The evolution of damage simulated by the cohesive surfaces here matches the indicators of damage onset behaviour seen in Fig. 5 and confirmed through SEM in Fig. 8.

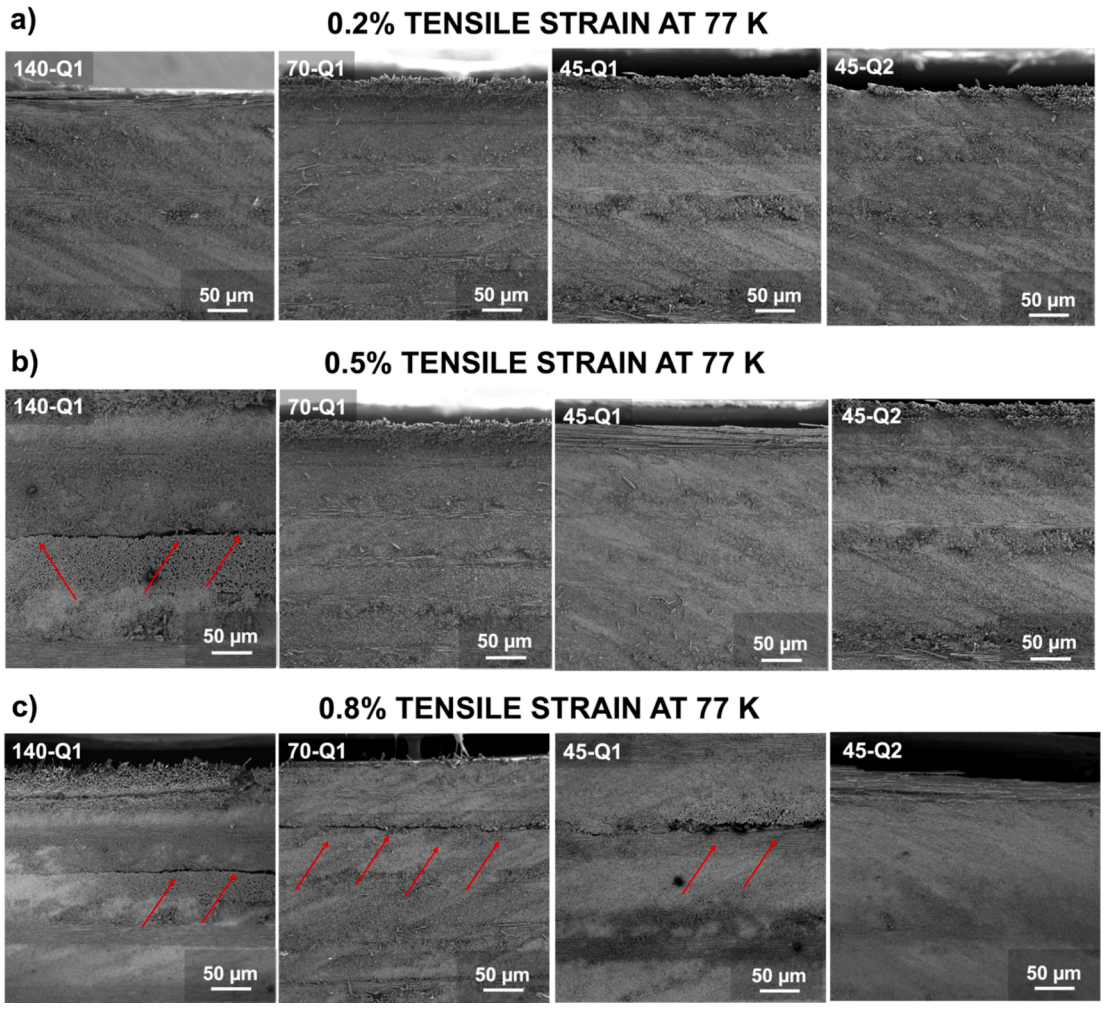

Fig. 8. SEM images of the cross-section surface of CEP-IMA laminates after tensile strain at 77 K, with at least 3 specimens for each strain level: a) 0.2 %, b) 0.5 %, and c) 0.8 %. Ply thickness and ply angle decrease from left to right.

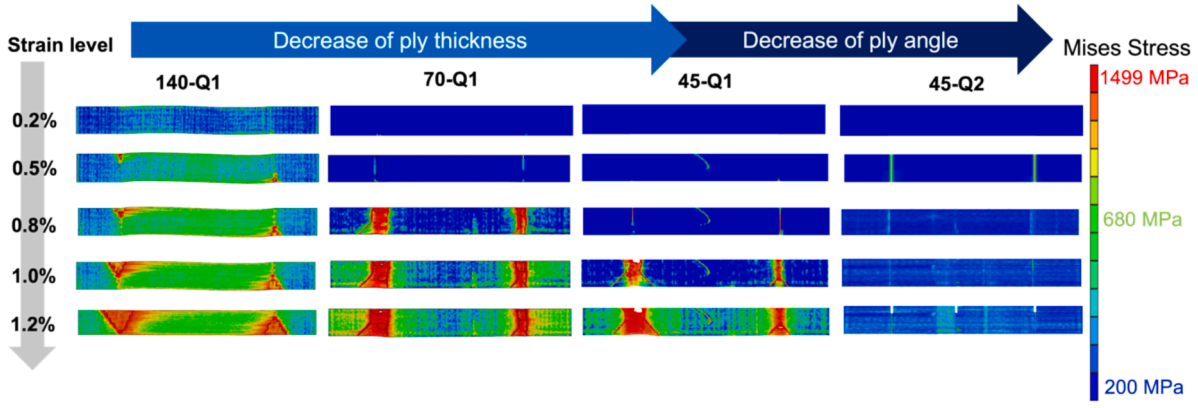

Fig. 9. Simulated cohesive element damage progression as a function of the strain at 77 K.

3.4.2. Damage and ultimate failure via whole specimen

In good qualitative agreement with the experimental behaviour seen at the tensile in-situ testing, decreasing the ply thickness and adding off-axis plies decreases significantly the residual stress and stress concentration levels at the CFRP laminate. Such a change spreads stress and damage into smaller and more dense concentrations throughout the plies, making the failure less likely to happen at the tabs where stress is localized. Instead, the sample behaves more similarly to a monolithic system. Fig. 10 exhibits a simulation analysis of the stress distribution comparison, from a whole-sample perspective, for all CFRP systems. Thicker ply laminates tend to have stress concentrations at the tabs and free edges. Reducing ply thickness helps distribute stress more evenly, allowing the laminate to withstand higher strain levels. This could reinforce the observed trend towards a monolithic failure mode, as illustrated in Fig. 6. Additionally, the graph shows that the lower ply-angled configuration Q2 improves performance by reducing residual

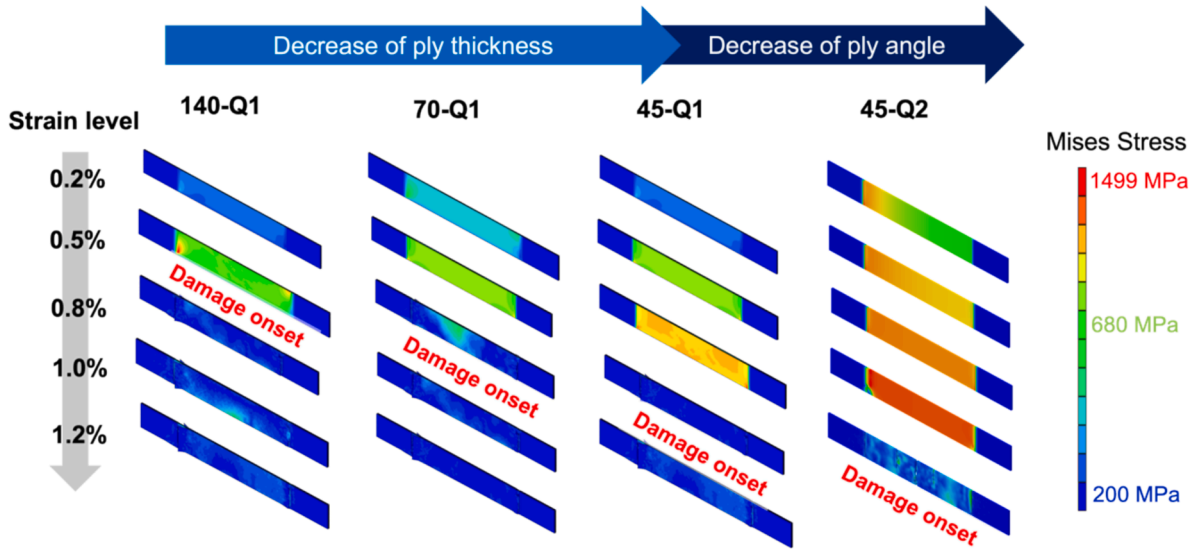

Fig. 10. Simulated stress distribution progression as a function of the strain at 77 K in a whole-sample observation.

stress from the testing temperature. The limited damage observed in thinner ply laminates is clearly reflected in the evolution of Mises stress values with the material's failure stress. Interestingly, the simulated stress levels align reasonably well with the experimental in-situ damage onset detected by signal shift (600–800 MPa). The fact that Mises stress was seen often shifted towards higher values indicates that the models were unable to fully capture the structural irregularities within the fiber–matrix distribution, particularly in thicker plies. However, the consistency in damage onset between the simulations and experiments indicates that some of the observed effects of ply thickness can be attributed to accurately representing the actual geometry, interfaces, and kinematics of the problem.

The stress–strain behaviour obtained from experimental measurements and FE simulations in 77 K environments was compared in Fig. 11. The focus here was on observing the similarity of the stress–-strain curves. Experimentally, reducing ply thickness improved stress–strain behaviour at failure, attributed to both crack size reduction and structural regularity, without affecting the elastic modulus. Thinner plies showed higher stress–strain failure, especially when transitioning

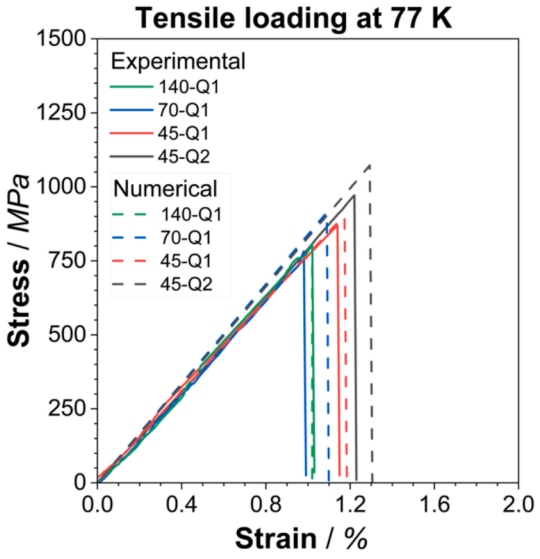

Fig. 11. Experimental and numerical comparison of tensile stress–strain curves at 77 K.

from 45-Q1 to 45-Q2 with off-axis plies. Numerically, the same trend was observed, with ultimate stress–strain failure increasing as ply thickness decreased. However, numerical results consistently overestimated experimental values, likely because they overlook the effect of the thin-ply manufacturing process. Despite this, the FE analysis demonstrated strong agreement with experiments, offering reliable insights for this study.

3.5. Leakage to damage relationship

The CEP-IMA material in the different ply thicknesses and stacking configurations is shown in Fig. 12**a** as the raw data of the leakage vs time. A small deviation in the magnitude of leakage rate is expected as samples vary in thickness and pressure difference. Thus, Fig. 12**b** exhibits the coefficient of permeability Φ, calculated according to **Eq. (6)**, at a plateau range (14 h), including the specimen leakage L, thickness t, permeation area A, and resulting pressure difference ΔP (see [39] for further details).

$$\Phi = \frac{p\ t}{\Delta P\ A} \tag{6}$$

Insignificant differences were observed in the values of the leakage measurements for unloaded and loaded specimens. The most notable case of deviation, seen in system 140-Q1, falls within the range of variation attributed to FVC and thus cannot be conclusively attributed to damage onset. This indicates that the thin plies effectively suppressed the formation of transverse matrix cracks, up to this load level, even at the point of delamination. Similar results were found for thin-ply CFRP materials tested in [5]. The onset of damage in these materials occurs as delamination rather than transverse microcracks. As observed in the SEM images (Fig. 8**c**), the laminates after 0.8 % strain were free of observable transverse microcracks, which are typically considered a primary source of leakage in the composite. Consequently, gas leakage occurs through the in-plane direction of the material along the circumference of the tank, making it undetectable on the opposite side of the CFRP wall. Transverse cracks, positioned perpendicularly to the wall, have a more substantial impact on the leakage of CFRP material. As mentioned in [3,4], a connected path of damage should increase the permeation levels in many orders of magnitude. Therefore, delamination damage is hereby insignificant (to some extent) regarding leakage. The findings of [5] also indicate that thin-ply (0°/90° crossply in this case) laminates could be loaded up to 1.4 % strain without significantly affecting the permeation of the CFRP material, which aligns with the

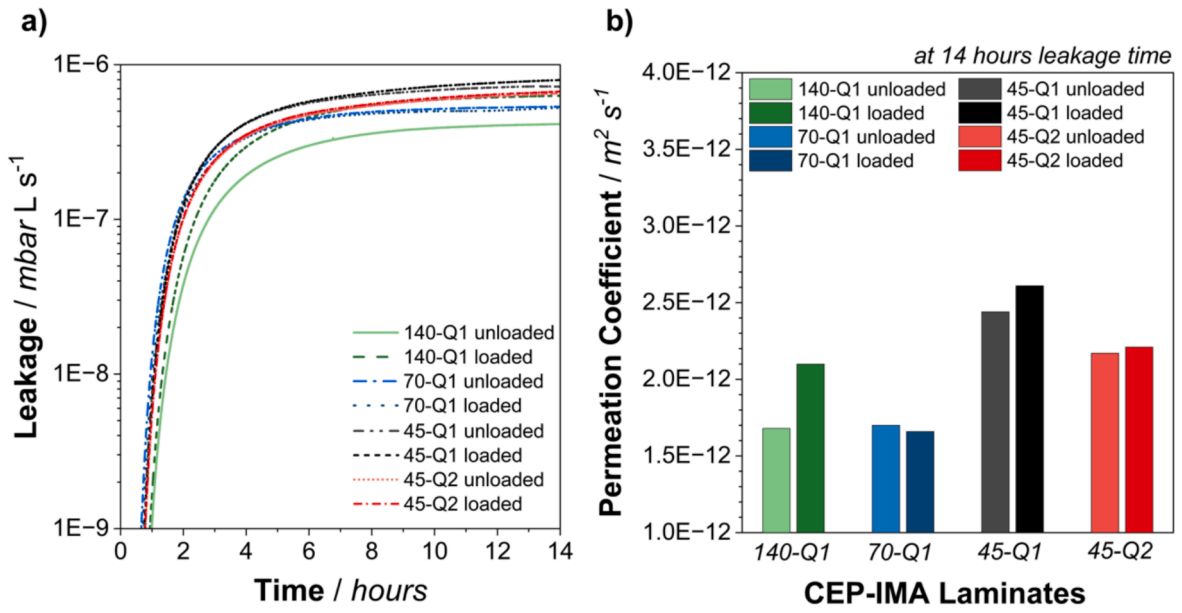

Fig. 12. Effect of pre-loading the CFRP laminates at 77 K up to 0.8 % strain on leakage as a) a raw leakage-time overview and b) a permeation coefficient at the time of 14 h.

results obtained in this study.

Finally, Table 4 summarizes a few values of permeation coefficient (or diffusivity) measured at RT reported in the literature for CFRP composites. Note that the values presented here were obtained under different experimental setups and conditions (such as gas type, pressure difference, etc.). Despite these variations and the inherent deviations in the data, the CFRP laminate studied here falls within the reported range for CFRP composites. Further studies and discussions on gas permeability in CFRP materials can be found in Saha and Sullivan [51].

4. Conclusions

This study investigated the effects of prepreg ply thickness and stack configuration on the tensile damage onset and ultimate failure of CFRP laminates in both RT and CTe environments. A method for detecting tensile damage onset testing while in LN2 was proven effective when combined with microscopy and simulation analysis. Additionally, providing a comprehensive survey of CFRP testing in cryogenic conditions is challenging, as factors like *in-situ* testing, damage analysis, FE simulation, and gas permeation are often studied separately. This work combines all these aspects, presenting a novel integrated approach. The findings here provide valuable insights into how these factors influence and are connected to the performance of CFRP composite laminates.

At 77 K, ultimate tensile properties such as modulus and strength are improved, while failure strain decreases slightly. At RT, ply thickness had minimal impact due to the ductile matrix compensating for manufacturing irregularities and plastic radius restriction in thicker plies. However, at CTe, these irregularities had a more significant influence. Reducing ply thickness from 140 to 45 g/m^2 enhanced ultimate failure stress and strain by 15 %, with an additional 25 % improvement seen in laminates with off-axis ply configurations Q2. Similarly, damage onset was significantly improved with thinner plies and lower ply angle orientations. Whereas 140-Q1 laminates showed early damage at 0.4–0.5 % strain at 77 k, thinner 70- and 45-Q1 laminates delayed damage onset to 0.7–0.8 %. The 45-Q2 laminate, with additional off-axis plies, exhibited steady behaviour without damage onset until composite failure at 1.2 % strain.

Subsequential microscopy analysis confirmed that delamination onset occurred earlier in thicker 140 gsm plies (0.5 % strain) compared to thinner 70 and 45 gsm plies (0.8 %). The 45-Q2 system, with off-axis plies, showed no signs of damage, consistent with strain curves lacking signal shifts associated with damage onset. Furthermore, FE simulations supported the experimental results, showing that reducing ply thickness and incorporating off-axis plies minimized stress concentrations and delayed the global damage initiation. This stress distribution reduced localized damage at the tabs and free edges, promoting a uniform and monolithic failure mode. Although the model has limitations, it captured the main effects of ply thickness on damage progression.

Finally, gas permeation tests revealed no significant increase in leakage levels after loading the systems to 0.8 % tensile strain at 77 K. Delamination damage was found to develop before transverse cracks, preventing significant leakage paths through the laminate thickness. Thus, delamination along in-plane fiber directions does not appear to compromise laminate leakage or the functionality of the LH2 storage concept.

In summary, this study demonstrates that optimizing prepreg ply thickness and stacking configuration can significantly enhance the tensile properties and damage onset resistance of CFRP laminates for cryogenic applications. The results highlight the importance of regular prepreg quality, reduced ply thickness, and well-designed stacking configurations for improving the performance of CFRP materials, especially when oriented to LH2 storage tanks. Future studies should investigate the impact of these parameters on the fatigue properties of these laminates in cryogenic environments, offering valuable insights into their behaviour under real-world conditions, particularly for LH2 tank applications.

Table 4
Comparison of permeation coefficient values for CFRP laminates of literature works.

Source	Material	Permeation Coefficient / $m^2\ s^{-1}$
Current study (CEP-IMA)	CFRP-epoxy $[0/45/90/135]_{2\text{-}5s}$	1.5–2.5 × 10^{-12}
Katsivalis et al. [5]	CFRP-epoxy [0/90/0/90/0]	5.2 × 10^{-12}
Flanagan et al. [49]	CFRP-PEEK $[45/135/0_4/135/45]$	5.2 × 10^{-11}
Condé-Wolter et al. [50]	CFRP-PA [UD]	2.9 × 10^{-13}

CRediT authorship contribution statement

Eduardo Szpoganicz: Writing – original draft, Investigation, Formal analysis, Data curation, Conceptualization. **Fabian Hübner:** Writing – review & editing, Validation, Supervision, Conceptualization. **Uwe Beier:** Writing – review & editing, Validation, Supervision. **Matthias Geistbeck:** Writing – review & editing, Validation, Supervision. **Maximilian Korff:** Writing – review & editing, Validation, Investigation. **Ling Chen:** Writing – review & editing, Validation, Software, Formal analysis. **Youhong Tang:** Writing – review & editing, Validation, Formal analysis. **Tobias Dickhut:** Writing – review & editing, Validation, Supervision. **Holger Ruckdäschel:** Writing – review & editing, Validation, Supervision.

Declaration of competing interest

The authors declare that they have no known competing financial interests or personal relationships that could have appeared to influence the work reported in this paper.

Acknowledgement

This project was carried out under the guidance of *Industrieanlagen-Betriebsgesellschaft mbH* (iABG) and financed by the Bavarian Ministry of Economic Affairs, Regional Development and Energy (STmWi) according to the registration number BLU-2109-0024.

Appendix A

For the simulation analysis conducted in this study, the material properties of the epoxy matrix (CEP), the carbon fibers (HexTow® IMA), and the composite laminate were employed based on data obtained from previous experimental studies in cryogenic environments. The specific properties used for each component are summarized in Table 5. Notice here, the properties of the carbon-fiber are provided by the technical datasheet and were not measured in CTe environments. However, considering the optimum molecular state of carbon-fibers, it is safe to consider insignificant change given by the CTe environment [3,4]. To address potential issues with model stiffness, the penalty stiffness values for the cohesive elements within the laminate were selected based on established guidelines of [52].

Table 5
Summarized properties of the matrix, fiber and their composite, utilized in this work for experimental and simulation analysis.

Properties measured in CTe environments	Value utilized for the simulation analysis
Matrix elastic modulus	3.4 GPa
Matrix critical stress intensity factor (K_{IC})	2.18 MPa $\sqrt{m}$
Matrix compression strength	400 MPa
Matrix tensile stress at failure	80 MPa
Matrix tensile strain at failure	3.7 %
Elastic modulus of the fiber (at RT)	296 GPa
Fiber stress at failure (at RT)	6067 MPa
Fiber strain at failure (at RT)	1.9 %
0° UD Laminate elastic modulus E_{11}	164 GPa
0° UD Laminate stress at failure	2400 MPa
0° UD Laminate strain at failure	1.24 %
90° UD Laminate elastic modulus E_{22}	11 GPa
90° UD Laminate stress at failure	70 MPa
90° UD Laminate strain at failure	0.8 %
Shear Modulus G_{12}	5.8 GPa
Interlaminar toughness mode I (G_{IC})	282 J m^{-2}
Interlaminar toughness mode II (G_{IIC})	733 J m^{-2}
Interlaminar shear strength (ILSS)	170 MPa
Interface shear strength (IFSS)	100 MPa
Coefficient of thermal expansion 0° UD	$-1.1\ \mu\ K^{-1}$
Coefficient of thermal expansion 90° UD	$53\ \mu\ K^{-1}$
Poisson's ratio ν_{12}	0.302
Poisson's ratio ν_{21}	0.066
X_t	1.83 GPa
X_c	1.34 GPa
Y_t	0.08 GPa
Y_c	0.21 GPa
S_{12}	0.11 GPa
S_{13}	0.11 GPa
S_{23}	0.08 GPa

Data availability

Data will be made available on request.

References

[1] International Energy Agency. Transport. Paris: IEA; 2022.
[2] Airbus official website – ZeroE program. https://www.airbus.com/en/innovation/low-carbon-aviation/hydrogen/zeroe, 2024 (accessed 05 July 2024).
[3] Z. Sápi, and R. Butler, 2020. Properties of Cryogenic and Low Temperature Composite Materials – A Review. Cryogenics 111 (October 2020). doi: 10.1016/j.cryogenics.2020.103190.
[4] Hohe J, Neubrand A, Fliegener S, Beckmann C, Schober M, Weiss K-P, et al. Performance of Fiber Reinforced Materials under Cryogenic Conditions – A Review. Comp Part A February 2021;141. https://doi.org/10.1016/j.compositesa.2020.106226.
[5] Katsivalis I, Signorini V, Ohlsson F, Langhammer C, Minelli M, Asp LE. Hydrogen Permeability of Thin-Ply Composites after Mechanical Loading. Compos A January 2024;176. https://doi.org/10.1016/j.compositesa.2023.107867.

[6] Chiao TT, Hamstad MA. Filament-Wound Kevlar 49/Epoxy Pressure Vessels. NASA Technical Reports Server September 2013;19790014039. https://ntrs.nasa.gov/citations/19790014039.

[7] G. H. Galiab, D. N. Kosareo, J. M. Roche. Cryogenic Composite Tank Design for Next Generation Launch Technology. Join Propulsion Conference and Exhibit 11-14th July 2004, Fort Lauderdale, Florida. (July 2004). https://arc.aiaa.org/doi/10.2514/6.2004-3390.

[8] Johnson WS, Pavlick MM, Oliver MS. Determination of Interlaminar Toughness of IM7/977-2 Composites at Temperature Extremes and Different Thicknesses. NASA Technical Reports Server May 2005;20050192417. https://ntrs.nasa.gov/citations/20050192417.

[9] Ju J, Morgan RJ. Characterization of Microcrack Development in BMI-Carbon Fiber Composite under Stress and Thermal Cycling. J Compos Mater November 2004;38(22):2007–24. https://doi.org/10.1177/0021998304044773.

[10] Gupta KS, Hojjati M. Moisture/Freeze/Dry Cycle, Thermal Cycling, Composites, Micro-Crack Initiation. International Journal of Composite Materials, no 2019;9:7–15. https://doi.org/10.5923/j.cmaterials.20190901.02.

[11] Timmerman JF, Hayes BS, Seferis JC. Cryogenic Microcracking of Carbon Fiber/Epoxy Composites: Influences of Fiber-Matrix Adhesion. J Compos Mater November 2003;37(21):1939–50. https://doi.org/10.1177/0021998303036281.

[12] Bechel VT, Kim RY. Damage Trends in Cryogenically Cycled Carbon/Polymer Composites. Compos Sci Technol September 2004;64(12):1773–84. https://doi.org/10.1016/j.compscitech.2003.12.007.

[13] M. Azeem, H. H. Ya, M. Azad Alam, M. Kumar, Z. Sajid, S. Gohari, et al., "Influence of winding angles on hoop stress in composite pressure vessels: Finite element analysis," Results in Engineering, vol. 21, 2024. doi: 10.1016/j.rineng.2023.101667.

[14] Li C, Qin Z, Li Y, Chen Z, Liu J, Liang J, et al. Investigation on mechanical behaviors under fatigue load of stacking sequences considering autofrettage process for highly reliable hydrogen storage vessel. J Storage Mater 2024;82:110538. https://doi.org/10.1016/j.est.2024.110538.

[15] Air A, Shamsuddoha M, Prusty BG. A review of Type V composite pressure vessels and automated fibre placement based manufacturing. Compos B 2023;253. https://doi.org/10.1016/j.compositesb.2023.110573.

[16] W. Wei, H. Rongjin, H. Chuanjun, Y. Zhao, S. Li, and L. Laifeng. Cryogenic Performances of T700 and T800 Carbon Fibre- Epoxy Laminates. IOP Conference Series: Materials Science and Engineering 102 (December 18, 2015): 012016. doi: 10.1088/1757-899X/102/1/012016.

[17] Hohe J, Schober M, Fliegener S, Weiss K-P, Appel S. Effect of Cryogenic Environments on Failure of Carbon Fiber Reinforced Composites. Compos Sci Technol August 2021;212:108850. https://doi.org/10.1016/j.compscitech.2021.108850.

[18] Hohe J, Schober M, Weiss K-P, Appel S. Validation of Puck's Failure Criterion for CFRP Composites in the Cryogenic Regime. CEAS Space Journal January 2021;13(1):145–53. https://doi.org/10.1007/s12567-020-00335-3.

[19] Szpoganicz E, Hübner F, Beier U, Geistbeck M, Ruckdäschel H. The Effect of Prepreg Ply Thickness in Carbon Fiber Reinforced Composites on Intralaminar Toughness and Shear Strength in Cryogenic Environments for Liquid Hydrogen Storage Tanks. Compos B 2024;253. https://doi.org/10.1016/j.compositesb.2024.112077.

[20] Li Y, Meng J, Luo J, Wang P, Zhao J, Lei H. Cryogenic Mechanics and Damage Behaviors of Carbon Fiber Reinforced Polymer Composites. Compos A June 2023;169:107484. https://doi.org/10.1016/j.compositesa.2023.107484.

[21] Gong M, Wang XF, Zhao JH. Experimental study on mechanical behavior of laminates at low temperature. Cryogenics 2006;46(7):445–51. https://doi.org/10.1016/j.cryogenics.2006.01.018.

[22] Grogan DM, Leen SB, Semprimoschnig COA, Brádaigh CMÓ. Damage characterisation of cryogenically cycled carbon fibre/PEEK laminates. Compos A 2014;66:237–50. https://doi.org/10.1016/j.compositesa.2014.08.007.

[23] Nair A, Roy S. Modeling of permeation and damage in graphite/epoxy laminates for cryogenic tanks in the presence of delaminations and stitch cracks. Compos Sci Technol 2007;67(11–12):2592–605. https://doi.org/10.1016/j.compscitech.2006.12.003.

[24] Meng J, Wang Y, Yang H, Wang P, Lei Q, Shi H, et al. Mechanical properties and internal microdefects evolution of carbon fiber reinforced polymer composites: Cryogenic temperature and thermocycling effects. Compos Sci Technol 2020;191:108083. https://doi.org/10.1016/j.compscitech.2020.108083.

[25] Hübner F, Brückner A, Dickhut T, Altstädt V, De Anda AR, Ruckdäschel H. Low Temperature Fatigue Crack Propagation in Toughened Epoxy Resins Aimed for Filament Winding of Type V Composite Pressure Vessels. Polym Test October 2021;102:107323. https://doi.org/10.1016/j.polymertesting.2021.107323.

[26] Hübner F, Hoffmann M, Sommer N, Altstädt V, Scherer A, Dickhut T, et al. Temperature-Dependent Fracture Behavior of Towpreg Epoxy Resins for Cryogenic Liquid Hydrogen Composite Vessels: The Influence of Polysiloxane Toughners on the Resin Yield Behavior. Polym Test September 2022;113:107678. https://doi.org/10.1016/j.polymertesting.2022.107678.

[27] Qu C-B, Wu T, Huang G-W, Li N, Li M, Ma J-L, et al. Improving Cryogenic Mechanical Properties of Carbon Fiber Reinforced Composites Based on Epoxy Resin Toughened by Hydroxyl-Terminated Polyurethane. Compos B April 2021;210:108569. https://doi.org/10.1016/j.compositesb.2020.108569.

[28] Sihn S, Kim R, Kawabe K, Tsai S. Experimental Studies of Thin-Ply Laminated Composites. Compos Sci Technol May 2007;67(6):996–1008. https://doi.org/10.1016/j.compscitech.2006.06.008.

[29] Amacher R, Cugnoni J, Botsis J. Thin Ply Composites: Experimental Characterization and Modeling. Composite Science and Technology September 2014;101:121–32. https://doi.org/10.1016/j.compscitech.2014.06.027.

[30] Furtado C, Arteiro A, Linde P, Wardle BL, Camanho PP. Is there a ply thickness effect on the mode I intralaminar fracture toughness of composite laminates? Theor Appl Fract Mech 2020;107:102473. https://doi.org/10.1016/j.tafmec.2020.102473.

[31] Furtado C, Tavares RP, Arteiro A, Xavier J, Linde P, Wardle BL, et al. Effects of ply thickness and architecture on the strength of composite sub-structures. Compos Struct 2021;256:113061. https://doi.org/10.1016/j.compstruct.2020.113061.

[32] Danzi F, Tavares RP, Xavier J, Fanteria D, Camanho PP. Effects of hybridization and ply thickness on the strength and toughness of composite laminates. J Compos Mater 2021;55(30):4601–16. https://doi.org/10.1177/00219983211041762.

[33] AhmadvashAghbash S, Broggi G, Aydemir A, Argyropoulos A, Cugnoni J, Michaud V, et al. Translaminar fracture in (non–)hybrid thin-ply fibre-reinforced composites: An in-depth examination through a novel mini-compact tension specimen compatible with microscale 4D computed tomography. Compos A 2025;188:108529. https://doi.org/10.1016/j.compositesa.2024.108529.

[34] 16459:. "Determination of the Fiber Volume Content of Fiber-Reinforced Plastics by Thermogravimetric Analysis (TGA)". .

[35] ASTM D3039. "Standard Test Method for Tensile Properties of Polymer Matrix Composite Materials". ASTM International.

[36] Jiang Q, Chen H, Chen L, et al. Experimental and Finite Element Simulation of Torsional Performance of Skin-core Carbon Fiber-reinforced Composite Rod. Appl Compos Mater 2023;30:1123–40. https://doi.org/10.1007/s10443-022-10090-9.

[37] A. P. C. Duarte, A. Díaz Sáez, and N. Silvestre. Comparative study between XFEM and Hashin damage criterion applied to failure of composites. Thin-Walled Structures, Volume 115, June 2017, Pages 277-288. doi: 10.1016/j.tws.2017.02.020.

[38] Chen L, Xing W, Chong J, Jiang Q, Ouyang Y, Wu L, et al. Understanding stiffness degradation of composite helical springs with multi-braided layers under impact. Compos A Appl Sci Manuf October 2024;185:108327. https://doi.org/10.1016/j.compositesa.2024.108327.

[39] ASTM D1434-82. "Standard Test Method for Determining Gas Transmission Rate Through Plastic Film and Sheeting". ASTM International.

[40] Camanho P, Dávila CG, Pinho ST, Iannucci L, Robinson P. Prediction of in Situ Strengths and Matrix Cracking in Composites under Transverse Tension and In-Plane Shear. Compos A February 2006;37(2):165–76. https://doi.org/10.1016/j.compositesa.2005.04.023.

[41] Catalanotti G. Prediction of in Situ Strengths in Composites: Some Considerations. Compos Struct January 2019;207:889–93. https://doi.org/10.1016/j.compstruct.2018.09.075.

[42] P. Maimí, E. González, and P. Camanho. Analysis of Progressive Matrix Cracking in Composite Laminates II. First Ply Failure. Journal of Composite Materials 48, no. 9 (April 2014): 1139–41. doi: 10.1177/0021998313483986.

[43] Flaggs DL, Kural H. Experimental Determination of the In Situ Transverse Lamina Strength in Graphite/Epoxy Laminates. J Compos Mater 1982;16(2):103–16. https://doi.org/10.1177/002199838201600203.

[44] Yamada SE, Sun CT. Analysis of Laminate Strength and Its Distribution. J Compos Mater July 1978;12:275. https://doi.org/10.1177/002199837801200305.

[45] H. M. Deuschle and B.-H. Kröplin. Finite element implementation of Puck's failure theory for fibre-reinforced composites under three-dimensional stress. Journal of Composite Materials, 46(19–20), 2485–2513. doi: 10.1177/0021998312451480.

[46] Dong H, Wang J, Karihaloo BL. An Improved Puck's Failure Theory for Fibre-Reinforced Composite Laminates Including the In Situ Strength Effect. Compos Sci Technol 2014;98:86–92. https://doi.org/10.1016/j.compscitech.2014.04.009.

[47] A. Wagih, P. Maimí, E.V. González, N. Blanco, J.R. Sainz de Aja, F.M. de la Escalera, R. Olsson, E. Alvarez. Damage Sequence in Thin-Ply Composite Laminates Under Out-of-Plane Loading. Composites: Part A 87 (2016): 66–77. doi: 10.1016/j.compositesa.2016.04.010.

[48] M. Flanagan, D.M. Grogan, J. Goggins, S. Appel, K. Doyle, S.B. Leen, C.M. Ó Brádaigh. Permeability of Carbon Fibre PEEK Composites for Cryogenic Storage Tanks of Future Space Launchers. Composites: Part A 101 (2017): 173–184. doi: 10.1016/j.compositesa.2017.06.013.

[49] J. Condé-Wolter, M.G. Ruf, A. Liebsch, T. Lebelt, I. Koch, K. Drechsler, M. Gude. Hydrogen Permeability of Thermoplastic Composites and Liner Systems for Future Mobility Applications. Composites: Part A 167 (2023): 107446. doi: 10.1016/j.compositesa.2023.107446.

[50] Saha S, Sullivan RW. A Review on Gas Permeability of Polymer Matrix Composites for Cryogenic Applications. J Compos Mater 2024;58(6):827–47. https://doi.org/10.1177/00219983241228550.

[51] Huang L, Tao Y, Sun J, Zhang D, Zhao J. Assessment of Numerical Modeling Approaches for Thin Composite Laminates Under Low-Velocity Impact. Thin-Walled Struct 2023;191:111053. https://doi.org/10.1016/j.tws.2023.111053.